

# JGR Biogeosciences











## RESEARCH ARTICLE

10.1029/2022JG007242

## Silicon Isotopes Highlight the Role of Glaciated Fjords in Modifying Coastal Waters

### Special Section:

Fjords: Estuaries on the Front-line of Climate Change

J. E. Hatton<sup>1,2</sup> , H. C. Ng<sup>2,3</sup>, L. Meire<sup>4</sup> , E. M. S. Woodward<sup>5</sup> , M. J. Leng<sup>6,7</sup> , C. D. Coath<sup>2</sup> , A. Stuart-Lee<sup>8</sup> , T. Wang<sup>2</sup> , A. L. Annett<sup>9</sup>, and K. R. Hendry<sup>2,10</sup> 

J. E. Hatton and H. C. Ng Joint first authorship.

### Key Points:

- Fjords have isotopically light dissolved silicon (DSi) in surface waters, despite an apparently rapid biological drawdown of DSi
- Silicon isotope geochemistry is a vital tool for disentangling complex fjord biogeochemical processes
- An isotopically light source of Si is responsible for modifying coastal waters within the fjords and beyond

### Supporting Information:

Supporting Information may be found in the online version of this article.

### Correspondence to:

J. E. Hatton,  
[jade.hatton@natur.cuni.cz](mailto:jade.hatton@natur.cuni.cz)

### Citation:

Hatton, J. E., Ng, H. C., Meire, L., Woodward, E. M. S., Leng, M. J., Coath, C. D., et al. (2023). Silicon isotopes highlight the role of glaciated fjords in modifying coastal waters. *Journal of Geophysical Research: Biogeosciences*, 128, e2022JG007242. <https://doi.org/10.1029/2022JG007242>

Received 19 OCT 2022  
Accepted 1 JUN 2023

<sup>1</sup>Department of Ecology, Charles University, Prague, Czechia, <sup>2</sup>School of Earth Sciences, University of Bristol, Bristol, UK, <sup>3</sup>Ifremer, Université Bretagne Occidentale, CNRS, Geo-Ocean, Plouzané, France, <sup>4</sup>Greenland Climate Research Centre (GCRC), Greenland Institute of Natural Resources, Nuuk, Greenland, <sup>5</sup>Plymouth Marine Laboratory, Plymouth, UK, <sup>6</sup>NERC Isotope Geosciences Facility, British Geological Survey, Nottingham, UK, <sup>7</sup>Centre for Environmental Geochemistry, School of Biosciences, University of Nottingham, Sutton Bonington Campus, Sutton Bonington, UK, <sup>8</sup>Department of Estuarine and Delta Systems, Royal Netherlands Institute for Sea Research, Yerseke, The Netherlands, <sup>9</sup>Ocean and Earth Science, University of Southampton, Waterfront Campus, National Oceanography Centre, Southampton, UK, <sup>10</sup>Polar Oceans Team, British Antarctic Survey, Cambridge, UK

**Abstract** Glaciers and ice sheets are experiencing rapid warming under current climatic change and there is increasing evidence that glacial meltwaters provide key dissolved and dissolvable amorphous nutrients to downstream ecosystems. However, large debate exists around the fate of these nutrients within complex and heterogenous fjord environments, where biogeochemical cycling is still often poorly understood. We combine silicon (Si) concentration data with isotopic compositions to better understand silicon cycling and export in two contrasting fjordic environments in south-west Greenland. We show that both fjords have isotopically light dissolved silicon (DSi) within surface waters, despite an apparently rapid biological drawdown of DSi with increasing salinity. We hypothesize that such observations cannot be explained by simple water mass mixing processes, and postulate that an isotopically light source of Si, most likely glacially derived amorphous silica (ASi), is responsible for further modifying these coastal waters within the fjords and beyond. Fjord to coastal exchange is likely a relatively slow process (several months), and thus is less impacted by short-term (<seasonal) changes of glacial meltwater input into the fjord, which has implications when considering the role of glacial meltwaters on nutrient export beyond the shelf break. We highlight the need for isotopic studies combined with dissolved and particulate nutrient concentration analysis to provide a more detailed analysis into the biogeochemical cycles within these highly dynamic fjord environments.

**Plain Language Summary** The Greenland Ice Sheet is melting at a faster rate than the global average as a result of climatic warming. The resulting meltwaters are known to contain essential nutrients, such as silicon, that can stimulate and support the growth of aquatic life in areas downstream to glacier catchments, particularly coastal environments such as fjords. However, the degree to which these glacial nutrients are transported through fjord environments is still highly debated. Furthermore, fjord environments are highly complex with competing biological and physical processes varying across time and space. We investigate two Greenlandic sites to disentangle the processes that govern the fate of glacier-sourced nutrient silicon in fjords. Our chemical analyses confirm the important role of reactive debris produced from glacier's physical grinding and chemical action on rocks under the ice sheet. We find evidence that the reactive debris continuously release nutrient silicon that is rapidly used by algae in fjords. Downstream transportation may provide a pathway for glacial nutrients to be transferred and used by marine life in the coastal and open ocean.

## 1. Introduction

The Arctic is experiencing some of the most rapid environmental changes as a result of global climatic change, with the Greenland Ice Sheet (GrIS) undergoing substantial mass loss. Arctic temperatures are rising at more than double the global average (Forster et al., 2021) and the significant ice mass loss from the GrIS has global implications via the impacts on oceanic circulation and biogeochemical cycles. Fjord environments act as the interface between the GrIS and the global ocean, largely influenced by increasing freshwater fluxes from land and marine terminating glaciers. Greenlandic glacial fjords are highly productive environments especially considering their

© 2023. The Authors.

This is an open access article under the terms of the [Creative Commons Attribution License](https://creativecommons.org/licenses/by/4.0/), which permits use, distribution and reproduction in any medium, provided the original work is properly cited.

cold temperatures, with pronounced increases in summer productivity attributed to glacial meltwater discharge (Grønkjær et al., 2019; Meire et al., 2017).

Glacial meltwaters have been shown to be a significant source of dissolved and amorphous silicon (DSi and ASi, respectively), with estimated fluxes of  $0.2 \text{ Tmol yr}^{-1}$  from the GrIS (Hawkings et al., 2017). Elevated Si concentrations have been reported on the inner shelves of Arctic coastal regions, due to the high Si fluxes exported from Arctic rivers (Carmack & Macdonald, 2004). Silicon is key for marine biochemical cycling and the global carbon cycle, by fueling siliceous primary producers such as diatoms. Recent studies have shown that spring diatom productivity in the Arctic Ocean is controlled by Si supply and limitation (Giesbrecht & Varela, 2021; Krause et al., 2019) highlighting the need to include glacially derived Si into regional climate models.

There has been a recent focus on understanding how fluxes of glacially derived nutrients impact downstream ecosystems, given that meltwaters are enriched in micro- and macro-nutrients (e.g., Hawkings, 2021; Hendry et al., 2019; Martin et al., 2020; Vick-Majors et al., 2020). However, the role of fjords in the modulation and drawdown of glacially derived nutrients is still poorly understood. Fjord environments are highly heterogeneous, with differences in hydrography, bathymetry and varying freshwater inputs all contributing differences in biogeochemical processes (Hopwood et al., 2019). Dissolved and particulate nutrient fluxes are largely influenced by circulation dynamics in fjord environments (Hopwood et al., 2015; Meire et al., 2016), and there is a significant biological uptake of nutrients in order to sustain spring and summer phytoplankton blooms (Meire et al., 2017). Glacial meltwaters strongly enrich surface fjord waters in DSi, with a 20%–160% increase of DSi expected into Greenland coastal regions by the end of the century (Meire et al., 2016). This will potentially increase diatom abundance in fjord environments, dependent upon nutrient stoichiometry within these environments with implications for carbon cycling in the region. There are marked differences in biogeochemical cycling and resultant productivity between fjord environments, particularly due to the differences in glacial meltwater inputs between fjords fed by land- and marine-terminating glaciers, particularly due to the upwelling of nutrient rich bottom waters by subglacial discharge in fjords with marine-terminating glaciers (Meire et al., 2017). Previous work has also suggested that glacial meltwaters impact coastal ecosystems beyond the fjord environment, with satellite observations and models suggesting that meltwater could impact phytoplankton blooms off south-west Greenland (Arrigo et al., 2017; Oliver et al., 2018). Furthermore, higher than expected diatom activities and elevated benthic fluxes off the west coast of Greenland in the Labrador Sea indicate rapid DSi cycling in these meltwater influenced coastal waters (Hendry et al., 2019).

Silicon is a useful tracer of glacial meltwaters in fjords and beyond, particularly when employing the combination of concentration and isotopic analysis. Silicon has three stable isotopes, and multiple biotic and abiotic processes within the fjord environment result in isotopic fractionation, alongside physical processes that shift isotopic values. Glacial meltwaters have a dissolved silicon isotopic composition (denoted by  $\delta^{30}\text{Si}_{\text{DSi}}$ ) that is, on average, lighter than non-glacial rivers (average  $+0.16\text{‰}$  compared to  $+1.38\text{‰}$ , respectively, Hatton et al., 2019a, 2019b). Glacial ASi has also been shown to be isotopically light, likely due to mechanochemical formation mechanisms within the subglacial system (Hatton et al., 2021), with average glacial amorphous silica isotopic values (denoted by  $\delta^{30}\text{Si}_{\text{ASi}}$ ) reported as  $-0.54\text{‰}$  ( $-0.85\text{‰}$  to  $-0.05\text{‰}$ , Hatton et al., 2019a, 2019b). Isotopic fractionation of Si occurs during the biological uptake of Si to biogenic silica (BSi) and abiological processes such as the formation of secondary weathering products (i.e., ASi) and the adsorption of Si onto iron and manganese oxide phases (Delstanche et al., 2009; Pickering et al., 2020). The changes in  $\delta^{30}\text{Si}_{\text{DSi}}$  within fjord systems, from glacial inputs to the fjord mouth and beyond the ocean shelf can therefore inform hypotheses on the biogeochemical processes and modification of waters in these environments.

There is a need to better understand the role of glaciated fjords in processing meltwaters to fully constrain how and when glacially derived nutrients may reach the coastal ocean and impact global nutrient cycles. To address this knowledge gap, we present biogeochemical data, including silicon isotopic data, from two contrasting fjord systems in south-west Greenland; Nuup Kangerlua (NK) and Ameralik Fjord (Figure 1). We present data from two years (June 2018 and September 2019) to compare and contrast the different processes occurring in both fjords with significantly different glacial inputs and hydrological systems. Our investigation of silicon isotope data from both fjords allows us to assess whether glacial waters biogeochemically modify coastal waters. Additionally, we can consider the impact of changing meltwater influences at differing times during the melt season on fjord silicon biogeochemical cycling. Finally, we combine silicon and radium isotopic data to determine the importance of these temporal differences in relation to the export timing from the fjord environment. This

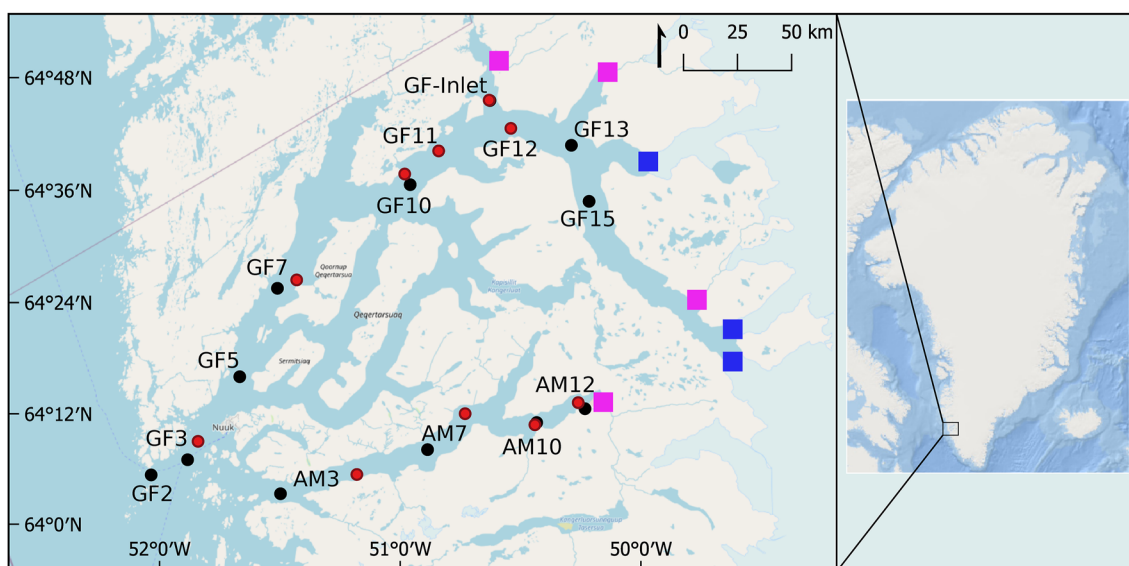


**Figure 1.** Map of sampling locations from July 2018 (red circles) and September 2019 (black circles) in Nuup Kangerlua (GF labeled stations) and Ameralik Fjord (AM labeled fjords). Purple squares highlight the location of glacial inputs from land-terminating glaciers and blue squares show glacial inputs from marine-terminating glaciers.

detailed investigation into silicon cycling of these two fjord environments via isotopic analysis will enable a better assessment into how these environments modify coastal waters and therefore will allow us to consider the exchange of glacially derived nutrients beyond the fjord system.

## 2. Materials and Methods

### 2.1. Sampling Locations

Sampling of NK (also commonly referred to as Godhåbsfjord (GF) in the literature) and Ameralik (AM) in south-west Greenland was carried out in July 2018 and September 2019 (Figure 1). Sampling was undertaken on board Greenlandic commercial vessels, MV Kisaq in July 2018 and MV Tulu in September 2019. Sampling locations approximately matched the stations regularly sampled by the Greenlandic Institute of Natural Resources (Mortensen et al., 2011) and we have followed the same station naming system for simplicity, hence will refer to stations by GF-“number” throughout the publication.

NK is one of the largest Greenlandic fjords by surface area (Mortensen et al., 2020), with a 190 km main fjord branch. It is fed by three marine-terminating glaciers (Kangiata Nunaata Sermia, Akullersuup Sermia, and Narsap Sermia) and proglacial rivers from three land-terminating glaciers (Qamanaarsuup Sermia, Kangilinnuata Sermia, and Saqqap Sermersua). It has a main sill depth of 170 m at the fjord mouth, with two further sills in-fjord at 250 and 277 m depth, within 47 km of the main sill (Mortensen et al., 2011). Sampling stations GF7 to GF15 lie upstream of these inner sills. This fjord system has been well-studied, with a range of data available for contextualizing our data; including circulation processes, biogeochemistry and nutrient export (e.g., Arendt et al., 2010; Juul-Pedersen et al., 2015; Meire et al., 2017; Mortensen et al., 2018).

In comparison, AM is less well studied with respect to biogeochemistry, with a detailed consideration of fjord hydrography only being completed recently (Stuart-Lee et al., 2021). AM is fed by one land-terminating glacier (via the river Naajat Kuuat) at the head of the fjord and non-glacial meteoric water sources. The main fjord is approximately 75 km long, with an area of around 400 km<sup>2</sup> (Stuart-Lee et al., 2021).

Upper coastal waters outside both fjords have a summer temperature around 0°C and salinity of 33 and are defined as Southwest Greenland CW, originating from the Arctic Ocean, traveling through the Fram Strait (Rysgaard et al., 2020). This upper layer is intermediately modified by colder, more saline water originating from Baffin Bay and the layer below is of Atlantic origin, which is warmer and more saline (Mortensen et al., 2022).

## 2.2. Sample Collection

A RBR concerto Conductivity, Temperature, Depth (CTD) profiler with cable attached Seapoint Tu sensor and Turner Cyclops chlorophyll fluorometer was deployed at each station. These CTD casts recorded depth profiles of conductivity, temperature, pressure, turbidity, and chlorophyll a (Chl-a) in continuous mode (Ruskin software v2.3.1, frequency 6 Hz). Data from the downcast only is reported, and the instrument was kept a minimum of 5 m above the bed to avoid sediment disturbance.

Surface (0–5 m) sampling was completed using a Towfish system, where acid-cleaned reinforced PVC tubing was attached to a plastic vane and weighed down with 24 kg of plastic-coated dive weights. Water was pumped onboard via a pneumatic Teflon bellows pump (A2CH1 F8 AstiPure II, Saint Gobain). Depth samples were collected using a 10 L Niskin bottle, with samples collected deepest to shallowest. Water for oxygen isotope ( $\delta^{18}\text{O}$ ) analysis was collected directly into acid-cleaned 30 ml HDPE bottles. Water for all other dissolved parameters was filtered via 0.2  $\mu\text{m}$  Acropak filter cartridge into acid-cleaned HDPE or LDPE bottles. Samples for nutrient analysis were frozen at  $-20^\circ\text{C}$  until analysis. Samples for stable silicon isotopes were kept refrigerated in the dark until analysis. Suspended sediments were collected by filtering a known volume of water via polycarbonate filters (0.22  $\mu\text{m}$ ) and stored frozen at  $-20^\circ\text{C}$  until analysis.

## 2.3. Laboratory Analysis

Inorganic nutrients ( $\text{NO}_3$ ,  $\text{NO}_2$ ,  $\text{PO}_4$ , and  $\text{Si}(\text{OH})_4$ ) were analyzed using a high resolution colorimetric 5-channel segmented flow autoanalyser at Plymouth Marine Laboratory, with analytical techniques reported by Woodward and Rees (2001), and by using the recognized GO-SHIP nutrient sample defrosting technique (Becker et al., 2020) prior to analysis. Typical uncertainty was 2%–3%.  $\delta^{18}\text{O}$  analysis was completed at the British Geological Survey (Keyworth) using the  $\text{CO}_2$  equilibration method. Internal standards were calibrated against international reference standards VSMOW2 and VSLAP2, with errors typically  $\pm 0.05\text{‰}$  (See Hendry et al. (2019) for full methodologies). Meltwater fractions were calculated using water  $\delta^{18}\text{O}$  composition and salinity mass balance, following the method outlined in Hendry et al. (2019) and references therein.

Dissolved stable silicon isotopes ( $\delta^{30}\text{Si}_{\text{DSi}}$ ) were measured at Bristol Isotope Group, University of Bristol. 0.22  $\mu\text{m}$  filtered samples were re-filtered in the laboratory via 0.02  $\mu\text{m}$  syringe filters (see Table S1 and Figure S1 in Supporting Information S1) prior to pre-concentration using Mg-induced co-precipitation (de Souza et al., 2012) and purification cation exchange resin (Biorad AG 50 W-X12, Georg et al. (2006)). Samples were analyzed using a Thermo Fisher Scientific™ Neptune multi-collector inductively coupled plasma mass spectrometer (MC-ICP-MS), using a dry plasma introduction system (Apex-IR). Standard-sample bracketing (NBS-28, NIST RM8546), intensity-matched Mg doping and  $\text{H}_2\text{SO}_4$  doping were used to correct for internal mass bias and anionic matrix mass bias (Georg et al., 2006; Hughes et al., 2011). Samples were measured in triplicate, where sample volume allowed, with an average external error of 0.12 $\text{‰}$  (2SD). Reference materials were analyzed alongside samples, with  $\delta^{30}\text{Si}$  Diatom reported as  $+1.26\text{‰} \pm 0.14\text{‰}$  ( $n = 43$ ) and LMG-08 reported as  $-3.46\text{‰} \pm 0.15\text{‰}$  ( $n = 50$ ), which agree well with published values. Additionally, seawater standard ALOHA<sub>1000</sub> was analyzed during each measurement session with an average value of  $+1.33\text{‰} \pm 0.16\text{‰}$  ( $n = 10$ ), which is in agreement with published values (Grasse et al., 2017). All standards and samples filtered via 0.02  $\mu\text{m}$  filters demonstrate mass dependent fractionation, with a gradient of 0.5119 for a three isotope plot (Figure S1 in Supporting Information S1, Reynolds et al., 2006).

Suspended sediments from polycarbonate filters were analyzed for amorphous and BSi concentrations (ASi + BSi, hereafter termed ASi) and  $\delta^{30}\text{Si}_{\text{ASi}}$ . Sequential leaching was used to determine ASi concentrations (Michalopoulos & Aller, 2004; Pickering et al., 2020), where  $\text{HO}_2\text{O}_2$  digestion of organic matter was followed by a HCl leach to remove authigenic minerals, then a  $\text{Na}_2\text{CO}_3$  extraction was completed following DeMaster (1981). Sediments were prepared for  $\delta^{30}\text{Si}_{\text{ASi}}$  analysis via a 0.2 M NaOH extraction (Hatton et al., 2019a, 2019b) and the subsequent solution was purified using cation exchange resin and analyzed using MC-ICP-MS, following the same methodology as dissolved samples. Unfortunately, the current common consensus of methodologies do not allow for ASi and BSi fractions to be separated and analyzed individually, preventing assessment of lability of the total ASi pool currently.

#### 2.4. Silicon Isotope Fractionation Model

We used a simple fractionation model (Varela et al., 2004) as a thought experiment to consider the in-fjord processes impacting the silicon isotope composition of surface waters. Closed (Equation 1) and open (Equation 2) models were run with a range of initial parameters and fractionation factors ( $\epsilon$ ) to consider a range of potential  $\delta^{30}\text{Si}_{\text{DSi}}$  when considering the role of diatom utilization in fjord waters, using an isotope mass balance approach.

$$\delta^{30}\text{Si}_{\text{seawater}} = \delta^{30}\text{Si}_{\text{initial}} - \epsilon \ln(f) \quad (1)$$

$$\delta^{30}\text{Si}_{\text{seawater}} = \delta^{30}\text{Si}_{\text{initial}} - \epsilon(1 - f) \quad (2)$$

Where;

$\delta^{30}\text{Si}_{\text{initial}}$  = prescribed set of initial conditions based upon either; 100% glacial, 100% seawater, or mixed conditions at 15 PSU.

$\epsilon$  = diatom fractionation factor.

$f$  = the remaining fraction of Si remaining when compared to the initial conditions.

Each model was run using three different fractionation factors ( $\epsilon$ ), based on the Si fractionation by various diatom species, including the commonly accepted average  $-1.1\text{‰}$ , plus specific  $\epsilon$  values for polar diatoms *Thalassiosira antarctica* ( $\epsilon = -0.74\text{‰}$ ) and *Thalassiosira pseudonona* ( $\epsilon = -1.21\text{‰}$ ), as reported by Sutton et al. (2013). These species were selected from the study by Sutton et al. (2013) as the *Thalassiosira* spp. characterize NK, making up an average of 73% of the community (Krawczyk et al., 2014), whereas the *Fragilariopsis* (also reported in Sutton et al. (2013)) is in much lower abundances in NK due to the relatively warm summer surface temperatures.

Initial conditions were varied to simulate source water from 100% glacial sources, 100% seawater source and a mixed source (a mix of glacial and seawater endmembers at 15 PSU). Glacial DSi concentrations and  $\delta^{30}\text{Si}_{\text{DSi}}$  values ranged from 20.7 to 49.4  $\mu\text{M}$  and  $-0.58\text{‰}$  to  $+0.51\text{‰}$ , respectively (Table S2 in Supporting Information S1). As there are no published data for glacial streams directly feeding NK or AM, we took values from a range of glacial rivers to best represent the potential variation in DSi concentration and  $\delta^{30}\text{Si}_{\text{DSi}}$  values from glacial rivers (Table S2 in Supporting Information S1, Hatton et al., 2019a, 2019b). Seawater values for initial conditions were derived from a range of values of outflow water from the Fram Strait. DSi concentrations ranged from 8.8 to 11.9  $\mu\text{M}$  and  $\delta^{30}\text{Si}_{\text{DSi}}$  values ranged from  $+1.64\text{‰}$  to  $+1.92\text{‰}$  (Table S3 in Supporting Information S1, Brzezinski et al., 2021). These values were selected as the CW outside of the two fjords originates mostly from Southwest Greenland CW, which originates via the Fram Strait (Rysgaard et al., 2020).

We compared the model simulations to a “Local Surface Seawater” value, which was measured in 2017 during the DY081 cruise close to the coast near the Nuuk fjords ( $63^{\circ}57'12.888''\text{N}$ ,  $-52^{\circ}55'0.5592''\text{W}$ ). The sample was taken at 1.3 m depth, with a DSi concentration of  $0.85 \pm 0.07 \mu\text{M}$  and  $\delta^{30}\text{Si}_{\text{DSi}}$  composition of  $+1.82\text{‰} \pm 0.2\text{‰}$ , so provides a useful comparison between surface waters within the fjord system and beyond the shelf break.

Surface  $\delta^{30}\text{Si}_{\text{DSi}}$  values from NK were also plotted in Figure 5 to compare to the model simulations. The  $f$  value was derived by calculating the Si remaining for each fjord sample compared to an average DSi concentration from the initial conditions of each model scenario. This varied for the three scenarios (100% glacial, 100% seawater and mixed source), as the DSi concentration of each set of starting conditions was dependent on the water source.

### 3. Results

#### 3.1. Hydro-Chemical Data

Both fjords show pronounced surface freshening in summer, resulting from the input of glacial meltwaters, with the lowest salinities in the upper 5 m closest to glacier outputs. NK has been well studied and our observations match well with previous sampling campaigns (e.g., Meire et al., 2017), with the inner fjord containing low salinity waters above 5 m depth, stratified from deeper, more saline waters by a pycnocline. Surface waters remain fresher further out-fjord in 2019 compared to 2018, likely due to the presence of icebergs in NK, in addition to the later season sampling and increased glacial melt throughout the summer prior to September sampling compared to July.



Surface water temperatures were warmer in 2018 compared to 2019 in both fjords, owing to the difference in sampling time between the two years. Water temperatures were also higher in AM compared to NK, particularly at the surface due to the addition of cold, fresh iceberg melt in NK.

It is important to note that GF-Inlet is not located within the main section of the fjord, but rather in a small fjord branch, with a shallow sill depth. This branch is fed by runoff from a land terminating glacier, which flows through Lake Tasersuaq before reaching the fjord branch. There was also substantial runoff entering the area from the steep valley sides of the fjord, potentially carrying large amounts of terrestrial material. The shallow nature of this site (maximum depth  $\sim 30$  m) and its location within a branch off the main section of the fjord, exhibits differing hydrological dynamics to the main fjord, and must be treated separately when considering the downstream export of material to the fjord mouth and beyond.

### 3.2. Dissolved Nutrients

Nutrient ratios highlight an excess of DSi relative to  $\text{NO}_3$  and  $\text{PO}_4$  in low salinity waters, where elevated DSi is being transported into the fjords by glacial meltwaters (Figure S3 and Table S4 in Supporting Information S1). However, the majority of samples where  $\text{NO}_3$ :DSi ratios fall below the 1:1 line are in surface waters, where diatom activity is expected to be minimal. Samples from the Chla-max (10–20 m deep) fall above the 1:1 ratio line and therefore  $\text{NO}_3$  is not assumed to be the limiting nutrient for diatoms. There is excess  $\text{PO}_4$  with respect to  $\text{NO}_3$  throughout the water column (Figure S3 in Supporting Information S1), which is also seen in other fjord systems (Santos-Garcia et al., 2022), due to the rapid uptake of  $\text{NO}_3$  by primary producers and the low  $\text{NO}_3$  concentrations contributed by glacial meltwaters.

Dissolved silicon (DSi) concentrations were highest in surface waters ( $<5$  m depth) further in-fjord for both fjords (Figure 2), with a significant positive correlation between DSi concentration and salinity in both fjords (NK;  $p = 3.4 \times 10^{-6}$ , AM;  $p = 1.1 \times 10^{-12}$ , Figure S2 in Supporting Information S1). There was a drawdown of surface DSi concentrations in both fjords toward the fjord mouth, which was more rapid in AM where there is only one point source of glacial meltwater at the head of the fjord (Figure 2). Low salinities, high DSi and high turbidity were recorded at AM12, but waters were already well-mixed with much higher salinity (31) by AM10. Surface DSi concentrations remained elevated in a large portion of NK until around GF7, owing to a greater volume of discharge from glacial sources.

Surface dissolved silicon isotope ( $\delta^{30}\text{Si}_{\text{DSi}}$ ) compositions were lightest in waters with lowest salinity and greatest glacial melt input in both fjords (Figures 2 and 3, Figure S4 in Supporting Information S1), likely owing to the isotopically light DSi signature expected from glacial meltwaters. The  $\delta^{30}\text{Si}_{\text{DSi}}$  values in both fjords fall below the simple water mass mixing line (Figure 4), highlighting a source of isotopically light DSi into both systems, which is discussed in further detail in Section 4.1. The deep water  $\delta^{30}\text{Si}_{\text{DSi}}$  values were similar in both fjords, with no significant differences between melt seasons. Unfortunately, no  $\delta^{30}\text{Si}_{\text{DSi}}$  data are available from the Chl-a max due to the low DSi concentrations and complex organic material leading to matrix interferences during analysis (Hughes et al., 2011).

Patterns of DSi concentrations and  $\delta^{30}\text{Si}_{\text{DSi}}$  were relatively similar across the two melt seasons in AM, with the highest DSi concentrations and the isotopically lightest composition at AM12 in both years, with a rapid drawdown of DSi by AM10 (Figure 2). The proportion of glacial meltwater reaching AM10 was greater in 2018 compared to 2019, with lower salinity, higher DSi, higher turbidity at AM10 in 2018 (Figures 2 and 3).

In comparison, in NK the glacial meltwater signature was evident further down fjord in 2019 compared to 2018. The glacial melt fraction at the surface was similar at GF12 and GF13 across both years, and the  $\delta^{30}\text{Si}_{\text{DSi}}$  composition of surface waters was similar ( $+0.54\text{‰}$  in 2018 and  $+0.38\text{‰}$  in 2019, Table 1). Whereas the glacial melt fraction was substantially lower at GF10 in 2018 when compared to 2019. This was accompanied by lower DSi concentrations at GF10 in 2018 and higher  $\delta^{30}\text{Si}_{\text{DSi}}$  composition in surface waters ( $+1.53\text{‰}$  in 2018 compared to  $+0.36\text{‰}$  in 2019).

### 3.3. Particulate Concentrations

Stations with the greater freshwater input also had higher turbidity concentrations at the surface, which is particularly evident in AM (Table 2). Waters at AM12 were extremely turbid during both 2018 and 2019 and had

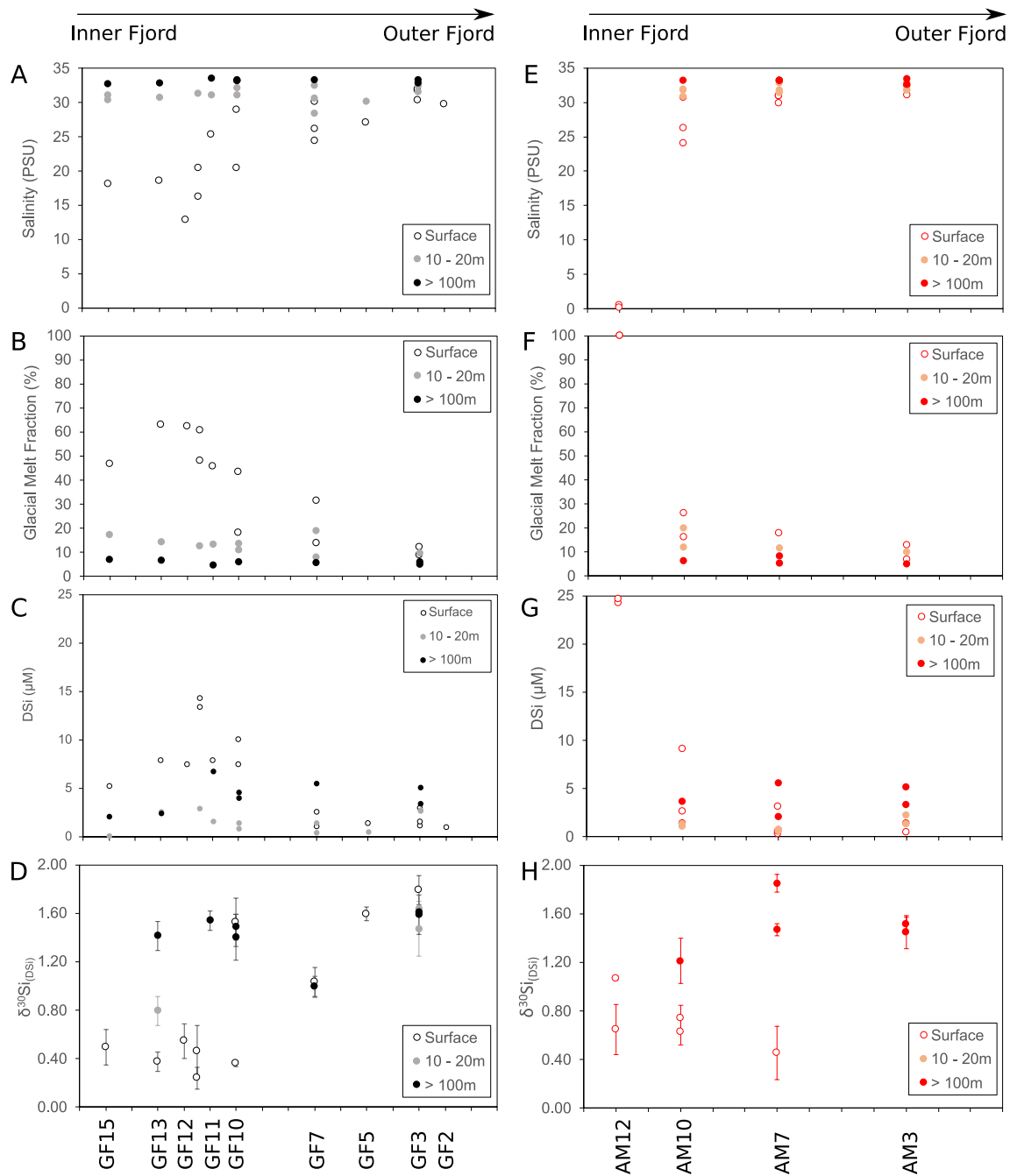


**Figure 2.** Scatter plots showing key dissolved geochemical parameters from (a–d) Nuup Kangerlua (NK) and (e–h) Ameralik Fjord (AM). Data from 2018 to 2019 is combined in each plot. Open circles represent surface data (>5 m), gray (NK) and orange (AM) circles represent samples taken from a depth of 10–20 m, and filled black (NK) and red (AM) circles represent deep water samples (>100 m).

correspondingly high ASi concentrations. ASi concentrations were higher at the surface and the Chlorophyll maximum (~15 m, based on fluorescence data) in AM in 2018 compared to 2019 at all stations, except for AM12. ASi concentrations generally decreased down-fjord at the surface and at the Chlorophyll maximum until a slight increase at AM3. In contrast, Chl-a concentrations increased down-fjord at the surface in AM in 2019 but peaked mid-fjord (AM7) at the Chl-a max. The highest Chl-a concentrations of AM were in 2018, at the inner fjord stations.

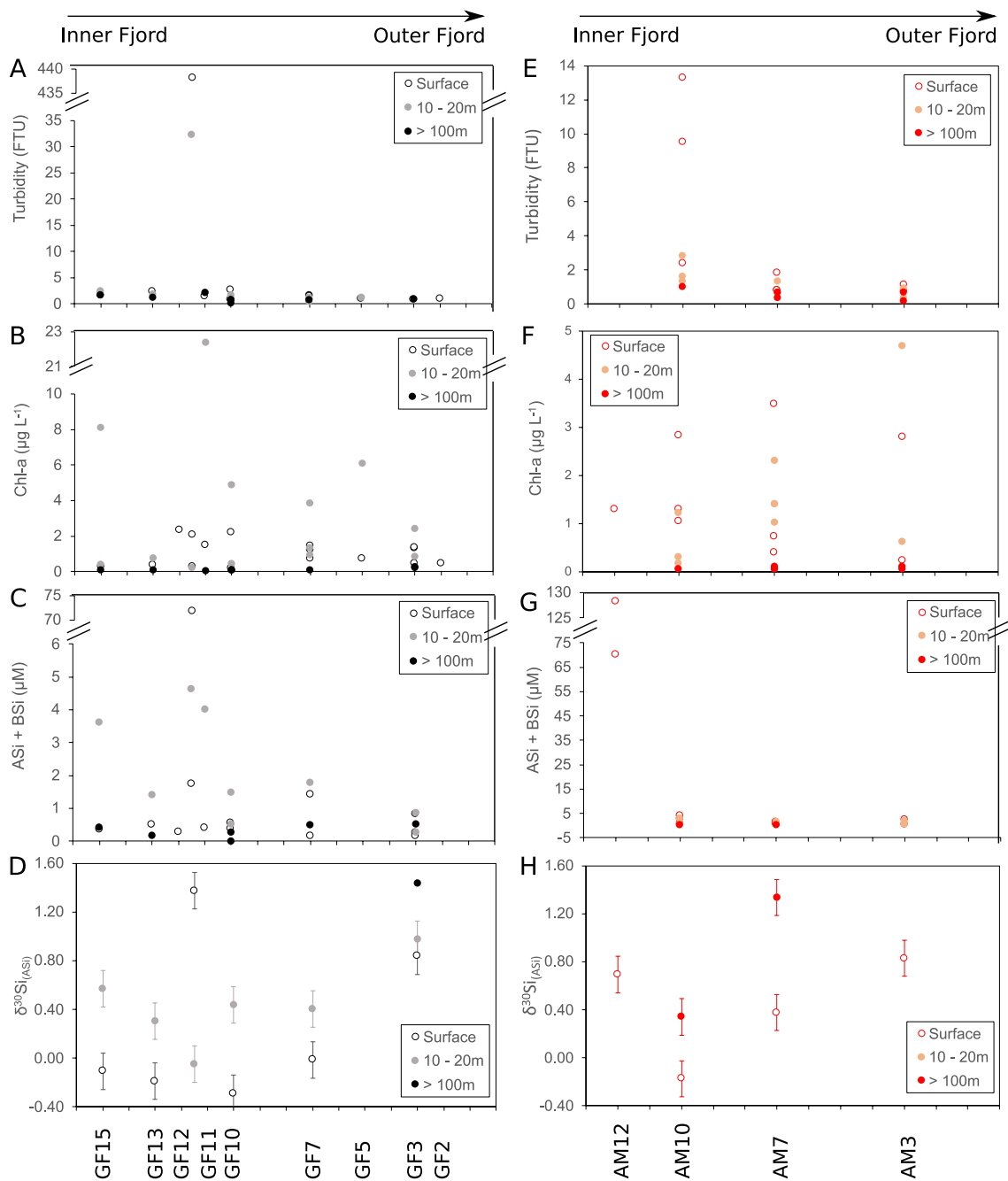


**Figure 3.** Scatter plots showing key particulate geochemical parameters from (a–d) Nup Kangerlua (NK) and (e–h) Ameralik Fjord (AM). Data from 2018 to 2019 is combined in each plot. Open circles represent surface data (>5 m), gray (NK) and orange (AM) circles represent samples taken from a depth of 10–20 m, and filled black (NK) and red (AM) circles represent deep water samples (>100 m). Note the different scales required for on the y-axis of the plots, due the differences between NK and AM.

The waters at GF11-Inlet in NK were extremely turbid in both 2018 and 2019, with elevated concentrations of ASI (Figure 3). In the main fjord trunk, ASI concentrations were highest at the Chl-a maximum at all stations, with the highest concentration at GF11 in 2018 and GF15 in 2019 (Figure 3). Elevated ASI concentrations coincided with elevated Chl-a concentrations in both years, with higher Chl-a concentrations generally in early summer samples (2018). Surface turbidity was elevated in 2019 compared to 2018 in NK, despite lower Chl-a concentrations in 2019, suggesting higher loads of abiotic suspended sediments coinciding with greater proportions of glacial melt in 2019.



**Table 1**

Summary of Key Surface (<5 m) Geochemical Parameters From Nuup Kangerlua in July 2018 and September 2019

| Station                                 | GF15  | GF13  | GF12 | GF-inlet | GF11 | GF10  | GF7   | GF5   | GF3   | GF2  |
|---|-------|-------|------|----------|------|-------|-------|-------|-------|------|
| <b>2018</b>                             |       |       |      |          |      |       |       |       |       |      |
| Salinity (PSU)                          | –     | –     | 12.9 | 20.5     | 25.4 | 29.0  | 30.2  | –     | 31.8  | –    |
| Turbidity (FTU)                         | –     | –     | –    | –        | 1.46 | 0.84  | 0.75  | –     | –     | –    |
| Glacial melt fraction (%)               | –     | –     | 62   | 48       | 46   | 18    | 14    | –     | 9     | –    |
| Chl-a ( $\mu\text{g L}^{-1}$ )          | –     | –     | 2.36 | 2.06     | 1.47 | 2.22  | 1.23  | –     | 1.34  | –    |
| DSi ( $\mu\text{M}$ )                   | –     | –     | 7.50 | 13.4     | 7.93 | 7.52  | 1.14  | –     | 1.23  | –    |
| ASi ( $\mu\text{M}$ )                   | –     | –     | 8.11 | 49.0     | 11.2 | 10.8  | 4.57  | –     | 7.35  | –    |
| $\delta^{30}\text{Si}_{\text{DSi}}$ (‰) | –     | –     | 0.54 | 0.46     | –    | 1.53  | –     | –     | –     | –    |
| $\delta^{30}\text{Si}_{\text{ASi}}$ (‰) | –     | –     | –    | –        | –    | –     | –     | –     | –     | –    |
| <b>2019</b>                             |       |       |      |          |      |       |       |       |       |      |
| Salinity (PSU)                          | 18.1  | 18.6  | –    | 16.2     | –    | 20.5  | 26.1  | 27.1  | 30.4  | 29.8 |
| Turbidity (FTU)                         | 1.56  | 3.26  | –    | 438      | –    | 2.68  | 1.36  | 0.93  | 0.82  | 0.91 |
| Glacial melt fraction (%)               | 47    | 63    | –    | 61       | –    | 43    | 31    | –     | 12    | –    |
| Chl-a ( $\mu\text{g L}^{-1}$ )          | 0.26  | 0.38  | –    | 0.30     | –    | 0.18  | 0.72  | 0.74  | 1.31  | 0.45 |
| DSi ( $\mu\text{M}$ )                   | 5.26  | 7.91  | –    | 14.3     | –    | 10.1  | 2.62  | 1.43  | 3.05  | 1.06 |
| ASi ( $\mu\text{M}$ )                   | 9.66  | 13.9  | –    | 2018     | –    | 15.2  | 39.6  | –     | 23.3  | –    |
| $\delta^{30}\text{Si}_{\text{DSi}}$ (‰) | +0.50 | +0.37 | –    | +0.24    | –    | +0.36 | +1.03 | +1.59 | +1.79 | –    |
| $\delta^{30}\text{Si}_{\text{ASi}}$ (‰) | –0.11 | –0.19 | –    | +1.37    | –    | –0.29 | –0.01 | –     | +0.84 | –    |

**Table 2**

Summary of Key Surface (<5 m) Geochemical Parameters From Ameralik Fjord in 2018 and 2019

| Station                                 | AM12  | AM10  | AM7   | AM3   |
|---|-------|-------|-------|-------|
| <b>2018</b>                             |       |       |       |       |
| Salinity (PSU)                          | 0.15  | 26.3  | 30.9  | 32.4  |
| Turbidity (FTU)                         | –     | 9.51  | 0.81  | 0.75  |
| Glacial melt fraction (%)               | 100   | 26    | –     | 6.8   |
| Chl-a ( $\mu\text{g L}^{-1}$ )          | 1.30  | 2.83  | 0.41  | 2.80  |
| DSi ( $\mu\text{M}$ )                   | 24.7  | 2.64  | 0.51  | 0.42  |
| ASi ( $\mu\text{M}$ )                   | 70.2  | 2.85  | 1.09  | 2.52  |
| $\delta^{30}\text{Si}_{\text{DSi}}$ (‰) | +1.07 | +0.63 | –     | –     |
| $\delta^{30}\text{Si}_{\text{ASi}}$ (‰) | –     | –     | –     | –     |
| <b>2019</b>                             |       |       |       |       |
| Salinity (PSU)                          | 0.5   | 30.7  | 29.9  | 31.0  |
| Turbidity (FTU)                         | –     | 2.38  | 1.82  | 1.14  |
| Glacial melt fraction (%)               | 100   | 16.1  | 17.9  | 12.7  |
| Chl-a ( $\mu\text{g L}^{-1}$ )          | –     | 1.06  | 0.74  | 0.23  |
| DSi ( $\mu\text{M}$ )                   | 24.2  | 1.34  | 3.10  | 1.37  |
| ASi ( $\mu\text{M}$ )                   | 128.2 | 0.78  | 0.59  | 13.9  |
| $\delta^{30}\text{Si}_{\text{DSi}}$ (‰) | +0.65 | –     | +0.45 | –     |
| $\delta^{30}\text{Si}_{\text{ASi}}$ (‰) | +0.69 | –0.17 | +0.37 | +0.83 |

The isotopic composition of ASi ( $\delta^{30}\text{Si}_{\text{ASi}}$ ) was analyzed in 2019 for NK and AM. The  $\delta^{30}\text{Si}_{\text{ASi}}$  values in surface waters were lower than at the depth of the Chl-a maximum and deep samples for all stations in NK, with the exception of GF-Inlet (Figure 3), highlighting the different source of suspended sediment material outside of the main fjord branch. The surface isotopic composition was lightest further in-fjord, coinciding with greater glacial melt percentage and increased toward to fjord mouth in both NK and AM. Deep water  $\delta^{30}\text{Si}_{\text{ASi}}$  values in AM were lower at AM10 compared to AM7, potentially highlighting the greater proportion of glacial particles settling closer to the glacial source, with a lighter isotopic composition.

## 4. Discussion

### 4.1. Modification of Coastal Waters

The role of glacial meltwaters in fjord biogeochemical cycling is still debated, with unanswered questions regarding the role of meltwaters in modifying coastal waters versus simple water mass mixing, especially considering the rapid drawdown of glacial nutrients in fjord environments. For example, glacial meltwaters have been found to enrich nearshore coastal waters with DSi (and other macronutrients) in an East Greenland fjord and the Canadian Arctic primarily through the stimulation of upwelling processes, supplying marine-sourced nutrients to the surface (Bhatia et al., 2021; Cape et al., 2019; Williams et al., 2021). We can use a combination of DSi concentrations and isotopic compositions to consider how saline and freshwater endmembers mix within these south-west Greenland fjord systems and assess the role of glacially derived Si within the fjord environment and beyond. DSi concentrations are highest in low salinity waters, with both fjords becoming depleted in DSi in surface waters toward the fjord mouth. Low DSi concentrations

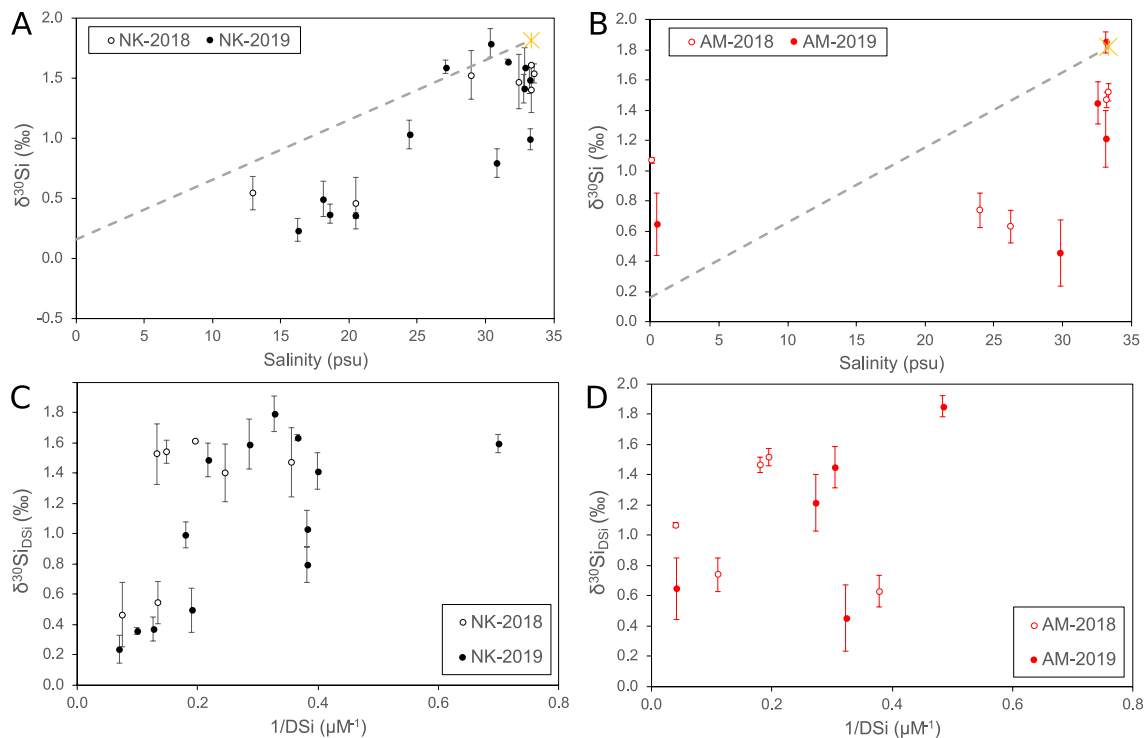


**Figure 4.** Scatter plots of dissolved silicon isotope composition (expressed as  $\delta^{30}\text{Si}_{\text{DSi}}$ ) for Nuuk Kangerlua (black) and Ameralik Fjord (red). Open circles represent data from 2018 and closed circles represent data from 2019. Errors represent 2 S.D. calculated from triplicate sample measurements where possible. If less than triplicate measurements were analyzed then an average sample and standard 2 S.D. value of  $0.12\text{‰}$  was used. Yellow stars in panels (a, b) represent the isotopic composition of surface waters at a seawater location sampled proximal to the fjords (depth = 1.3 m), with 2 SD error included within the size of the symbol. Gray dotted lines in panels (a, b) represent simple mass mixing lines between an average glacial meltwater  $\delta^{30}\text{Si}_{\text{DSi}}$  composition (Hatton et al., 2019a, 2019b) and the measured local surface seawater  $\delta^{30}\text{Si}_{\text{DSi}}$  composition.

toward the fjord mouth are not unexpected considering the degree of vertical stratification and biological uptake, combined with limited lateral flux of nutrient-rich glacial meltwater down-fjord and mixing of surface coastal waters low in DSi (Mortensen et al., 2020). This is particularly true of NK, which is a highly productive fjord, with spring and summer phytoplankton blooms directly impacting elevated productivity in higher trophic levels throughout the summer period (Meire et al., 2017). Diatoms account for up to 90% of primary producer biomass in NK (Meire et al., 2016), due to the high DSi availability, thus the low DSi concentrations down-fjord can be largely attributed to biological uptake, particularly considering strong spring bloom activity within this fjord (Meire et al., 2017). The conversion of DSi to BSi via diatom uptake leads to isotopic fractionation, with resultant BSi enriched in lighter Si isotopes, due to the preferential uptake of  $^{28}\text{Si}$  by diatoms. The residual fjord waters therefore have lower DSi concentrations, with a higher  $\delta^{30}\text{Si}_{\text{DSi}}$  value.

Therefore, if water mass mixing was conservative within the fjord environment and diatom uptake of DSi to BSi was the key biogeochemical process occurring, then we could expect the  $\delta^{30}\text{Si}_{\text{DSi}}$  composition of fjord waters to increase as DSi concentration decreased concomitant with increasing salinity. While there is a positive relationship between  $\delta^{30}\text{Si}_{\text{DSi}}$  values and salinity (Figure 3), we can demonstrate that the  $\delta^{30}\text{Si}_{\text{DSi}}$  composition of fjord waters is too low to be explained by a combination of simple water mass mixing and biological uptake of DSi (Figure 4). Oceanic waters likely feeding into the fjords around Nuuk have a similar  $\delta^{30}\text{Si}_{\text{DSi}}$  composition to surface fjord waters in NK, but they are elevated in DSi concentration compared to NK. The Southwest Greenland CW feeds the fjords sampled in this study and this water mass flows via the Fram Strait Outflow (Rysgaard et al., 2020), which has  $\delta^{30}\text{Si}_{\text{DSi}}$  values of between  $+1.64\text{‰}$  and  $+1.92\text{‰}$  and DSi concentration of 8–12  $\mu\text{M}$  (Brzezinski et al., 2021). Similarly, waters from the Labrador Sea at a depth of 499 m (Geotraces Station 64, Sutton et al., 2018) has a  $\delta^{30}\text{Si}_{\text{DSi}}$  value of  $+2.01\text{‰}$  and DSi concentration of  $\sim 8 \mu\text{M}$ . Meanwhile, a local surface seawater site proximal to the Nuuk fjords was reported to have  $\delta^{30}\text{Si}_{\text{DSi}}$  composition of  $+1.82\text{‰}$ , but a low DSi concentration of only  $0.85 \mu\text{M}$  (see methodology). These values are similar to those at the outer NK fjord stations GF5 and GF7, with  $\delta^{30}\text{Si}_{\text{DSi}}$  composition of  $+1.59\text{‰}$  and  $+1.79\text{‰}$ , respectively and DSi concentrations of less

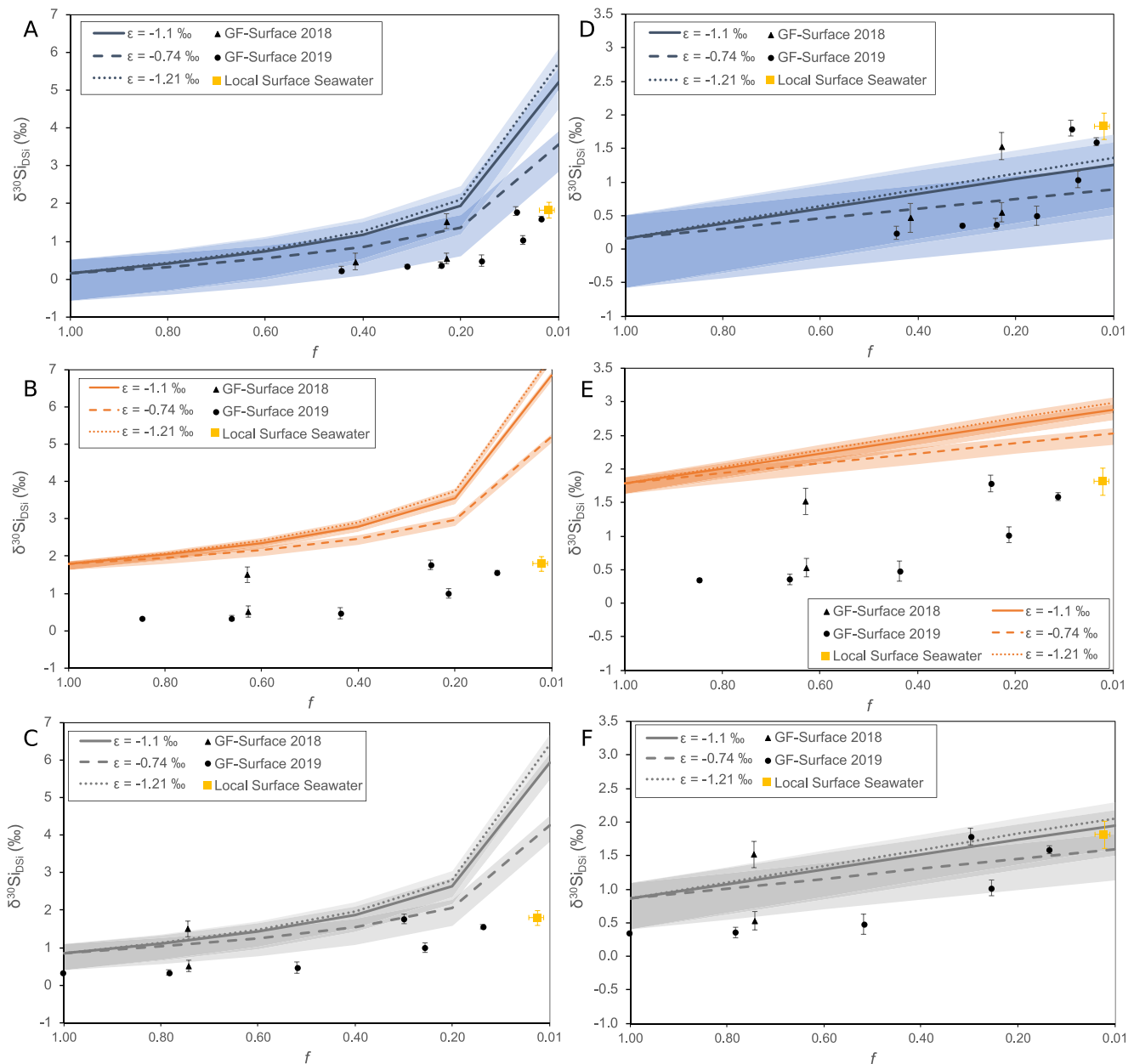


**Figure 5.** Plots showing outputs from (a–c) closed to (d–f) open system Fractionation Model (based on Varela et al. (2004)). Black circles in all plots represent actual observed silicon isotopic composition from Nuup Kangerlua in 2018 and 2019. Yellow circle is the isotopic composition from surface seawater in a proximal location to the sampled fjords. Each line is a result of the model with different fractionation factor (solid =  $-1.1‰$ , dashed =  $-0.74‰$ , and dotted =  $-1.21‰$ ). Shaded areas show model uncertainty when a range of starting endmember values were used (see Supporting Information S1 for further information). (a, d) Blue lines use 100% glacial endmembers as starting conditions, (b, e) orange lines use 100% seawater endmember conditions, and (c, f) gray lines use a mixed glacial-seawater endmember with a starting salinity of 15.

than  $3.1 \mu\text{M}$ . Considering the DSi higher concentrations of potential seawater endmembers (e.g., Southwest Greenland CW) entering NK, we can assert that processes beyond simple water mass mixing are occurring to account for lower concentrations of DSi in surface and 10–15 m of fjord waters. The lower DSi concentrations along fjord do suggest biological uptake by primary producers, but the surface water  $\delta^{30}\text{Si}_{\text{DSi}}$  values suggest additional processes must also be occurring to maintain a relatively light isotopic composition.

Whilst drawdown of glacial waters is clearly much faster in AM, based on the steep salinity and DSi gradients at the head of the fjord, the same hypotheses can also be used to explain the patterns in  $\delta^{30}\text{Si}_{\text{DSi}}$  values. Surface waters contain isotopically light DSi after the increase in salinity and decrease in DSi concentrations, in both

2018 and 2019 (Stations AM10 and AM7, Figure 4b), suggesting that the initial drawdown of DSi was not simply biological uptake or secondary weathering formation, as this would have been accompanied by an increase in  $\delta^{30}\text{Si}_{\text{DSi}}$ . Therefore, despite clear differences in fjord dynamics as a result of the differing glacial inputs (e.g., Meire et al., 2017), the same process supplying isotopically light Si may be occurring in both fjords in order to explain the decrease in DSi concentrations and while  $\delta^{30}\text{Si}_{\text{DSi}}$  values also remain low.

We can further demonstrate the requirement of an isotopically light source of Si to explain the  $\delta^{30}\text{Si}_{\text{DSi}}$  variation within surface waters in NK by conducting a simple thought experiment via a basic fractionation model (modified from Varela et al. (2004)). Here we model the drawdown of Si via diatom utilization, taking into account a range of biological isotopic fractionation factors and endmembers for glacial and seawater isotopic composition (see methodology for details). We have considered both scenarios where (a) biological uptake rates greatly exceed the rate of DSi input resulting in an essentially “closed” system, or (b) where DSi input rates are sufficiently high to result in an isotopically “open” system. Neither system reflects the complexity of the fjord surface, and it is likely that the environment represents a dynamic hybrid of “open” and “closed” systems that is heterogeneous in space and time, depending on numerous factors for example, water column stratification due to freshwater input and the upwelling of nutrients via subglacial discharge (Stuart-Lee et al., 2021). Instead, the purpose of this two-endmember model is to highlight that complex, non-conservative processes have to be occurring in order to explain the isotopic composition of DSi, rather than pseudo-conservative mixing behaviors in surface waters (Hopwood et al., 2019). We have modeled the  $\delta^{30}\text{Si}_{\text{DSi}}$  composition of surface waters using three fractionation factors for diatom uptake. It is commonly accepted that the fractionation factor for diatom uptake ( $\epsilon$ ) is  $-1.1\text{‰}$  (de la Rocha et al., 1997). However, diatom fractionation has been shown to be species dependent (Sutton et al., 2013), so we have therefore considered a range of  $\epsilon$  from  $-1.21\text{‰}$  to  $-0.71\text{‰}$  to reflect the likely dominance of polar species. We use a range of starting conditions, where we consider the  $\delta^{30}\text{Si}_{\text{DSi}}$  composition if the Si input is solely glacially sourced, seawater-sourced or a mixed source (with a salinity of 15 PSU, which equates to approximately 57% glacial input). In the closed system scenarios (Figures 5a–5c), the model is unable to recreate the local surface seawater isotopic composition regardless of whether starting conditions reflect 100% glacial water (Figure 5a), 100% seawater (Figure 5b) or a mixed composition of glacial and seawater (Figure 5c): in all scenarios, the model-derived  $\delta^{30}\text{Si}_{\text{DSi}}$  is heavier than the observed value at the corresponding DSi concentrations. This suggests a source of light DSi into the fjord surface waters is missing from the model. The open system model is more successful in replicating observed data, particularly scenarios where the starting water mass is 100% glacial (Figure 5d) and a mixed water source with a salinity of 15 (Figure 5f). The 100% seawater open system scenario (Figure 5e) still fails to produce  $\delta^{30}\text{Si}_{\text{DSi}}$  values as low as the observations, highlighting that there must be influence from glacial meltwater within the fjord environment and out into the coastal waters to explain the observed  $\delta^{30}\text{Si}_{\text{DSi}}$  data. Whilst there is upwelling of deep, nutrient rich bottom-waters in near the terminus of marine-terminating glaciers, this is unlikely to impact the surface waters much further down fjord, especially due to biological uptake. This means that the open system model is probably less likely to be successfully replicating the true surface processes at the lower DSi concentrations within the model.

The models with starting conditions of 100% glacial meltwater are unlikely scenarios, as the proportion of meltwater in the fjord environment usually much lower, simply due to water mass mixing. There is clearly glacial meltwater input into the fjords, so the 100% seawater endmember is also an unrealistic scenario. However, it is useful to highlight these extreme scenarios to consider what potential inputs would be required to reach the observed  $\delta^{30}\text{Si}_{\text{DSi}}$  values in NK. The 15 PSU endmember requires 57% glacial meltwater and glacial melt fractions over 50% are only recorded in surface waters in NK at GF13 (Table 1), which is in close proximity to a glacial outlet, so this is an unlikely scenario for fjord waters further down fjord where the proportion of glacial water is much lower. Even despite the high glacial influence, the 15 PSU model is unable to recreate the observed  $\delta^{30}\text{Si}_{\text{DSi}}$  values in the closed system model (Figure 5b), particularly the local seawater endmember from just outside the fjord system. This model performs better for using open system configuration, however it is unlikely that there is enough DSi replenishment in the true fjord environment for this model to be considered realistic. Given that non-glacial riverine input would be isotopically heavier than glacial input (Hatton et al., 2019a, 2019b), any change in the freshwater isotopic composition in the model would worsen the mismatch with observations. By using these simple models to consider the fate of DSi and associated isotopic composition with biological uptake in the fjord environment, we can hypothesize that there is a clear modification of coastal waters, with a source of isotopically light DSi contributing to the Si cycling within the water masses. We postulate that the observed  $\delta^{30}\text{Si}_{\text{DSi}}$  composition in both NK and AM cannot be explained by simple water mass mixing, as more complex

modification of fjord biogeochemistry by glacial meltwaters must be occurring to explain the silicon cycling in these fjords.

In order to balance the isotopic fractionation associated with biological uptake of DSi in these fjords, there must be another source of Si that undergoes dissolution, with a light isotopic composition. We suggest a reactive form of particulate Si is influencing the  $\delta^{30}\text{Si}_{\text{DSi}}$  values within surface waters. Sediment efflux has been shown to be a significant source of DSi in the region (Ng et al., 2020), which could help to explain some of the elevation in particulate concentrations combined with isotopically light DSi. However, porewater  $\delta^{30}\text{Si}_{\text{DSi}}$  values in glaciated fjords are generally very high (Ng et al., 2022). Therefore, the most realistic explanation remains the dissolution of isotopically light ASi, derived from glacial meltwaters. Glacially derived ASi from a range of glaciers has been shown to be enriched in  $^{28}\text{Si}$ , with an average  $\delta^{30}\text{Si}_{\text{ASi}}$  composition is  $-0.39\text{‰}$  (range:  $-0.01\text{‰}$  to  $-0.86\text{‰}$ , Hatton et al., 2019a, 2019b). It is most plausible that DSi uptake by diatoms is occurring concurrently with the dissolution of isotopically light ASi, thus the overall DSi concentration remains low. Dissolution of this ASi in the surface fjord environment would lead to the maintenance of lower  $\delta^{30}\text{Si}_{\text{DSi}}$  values, despite the uptake and resultant fractionation of DSi by diatoms. Hawkings et al. (2017) demonstrated the potential for rapid dissolution of glacial ASi across the salinity gradient via leaching experiments, highlighting the potential for such material to impact biogeochemical cycles. We recognize that not all fjord environments show the high dissolution potential as seen by Hawkings et al. (2017), with an average Si enrichment of 13% found from a range of glacial fjords (Hopwood et al., 2020). However, only a relatively small fraction of overall glacial ASi would be required to undergo dissolution in order to impact the overall isotopic composition of surface waters, considering average ASi concentrations of  $58\ \mu\text{M}$  (Hatton et al., 2019a, 2019b). As a further thought experiment, we can consider the proportion of ASi required to undergo dissolution in NK surface waters to close the isotope balance between the modeled and observed  $\delta^{30}\text{Si}_{\text{DSi}}$  values. We show the concentration of ASi required for the open and closed models with mixed water (15 PSU) are realistic considering likely ASi dissolution (Table S5 in Supporting Information S1). Between 1.6 and  $18.1\ \mu\text{M}$  of ASi is required for the closed system model and between 0.2 and  $14.7\ \mu\text{M}$  of ASi for the open system model (for a fractionation factor of  $-1.1\text{‰}$ ). This equates to 2.8%–31% and 0.04%–25% of the average ASi concentrations measured from a range of glacial catchments (Hatton et al., 2019a, 2019b), which is a realistic amount of dissolution, given the rapid dissolution potential with increasing salinity (Hawkings et al., 2017). We postulate that this dissolution would be accompanied by concurrent diatom utilization, leading to a cycling of DSi concentration and  $\delta^{30}\text{Si}_{\text{DSi}}$  composition change, thus a couple biogeochemical model of fjord environments is key to fully consider a robust prediction of these complex, highly dynamic environments.

It is also possible that desorption of Si from reactive iron and manganese phases that originate from subglacial sediments could also release isotopically light DSi into the water. Given adsorption results in very strong fractionation, preferentially taking up the lighter Si isotopes (Delstanche et al., 2009; Pickering et al., 2020; Ward et al., 2022), release of this Fe (and Mn)-bound Si could have a significant impact on surface water isotopic composition. Abiotic desorption or inorganic phosphorus is observed in estuarine environments and experimental processes (Deborde et al., 2007), with an increase in dissolved inorganic phosphorus along the salinity gradient and we could expect Si to behave in a similar way. However, more work is required to identify and quantify such Si desorption processes with estuarine environments, especially because this mechanism holds a potentially important source of isotopically light DSi for these systems.

By using a combination of concentration and isotopic data we highlight the requirement of glacial waters to modify coastal waters within these fjord environments, thus providing evidence of the importance of glacial meltwater export on biogeochemical cycling within and beyond the fjord environment in both land- and marine-terminating glacier fjords.

## 4.2. Coastal Exchange Timescale More Important Than Early and Late Summer Changes

### 4.2.1. Subtle Changes in Si Biogeochemistry Between Early and Late Summer

Silicon isotopic data strongly suggest a large influence of glacial meltwater in modifying coastal waters, thus the timing of glacial melt export into the fjords could have a significant influence on biogeochemistry in the region. Studying both fjords at two different points in the melt season allowed us to assess any differences in the processes impacting biogeochemical cycling and glacial melt impact between early and late summer. Seasonal evolution of fjord ecosystems has been documented previously, via spring and summer blooms for example,



(Meire et al., 2017). Therefore, we expected to document differences in the biogeochemistry of the fjord waters between July and September, particularly in the more productive NK. A glacial meltwater fingerprint, based on the light isotopic composition in surface waters, was observed further out-fjord in 2019 in NK compared to 2018 (Table 1, Figure 3a), with surface  $\delta^{30}\text{Si}_{\text{DSi}}$  values similar at GF10 in July compared to GF5 in September. This is the opposite to what may be expected, with cumulatively more biological uptake by September, after the summer bloom, compared to June when samples were collected in 2018. However, the lower  $\delta^{30}\text{Si}_{\text{DSi}}$  composition further out fjord is likely explained by the greater cumulative meltwater discharge by September, and delivery of isotopically light DSi and ASi, providing support for the importance of glacial waters modifying the fjord biogeochemistry. In addition, a larger proportion of the freshwater signal in July is likely attributed to snowmelt, rather than glacial meltwaters routed via the subglacial environment. This freshwater source would not be expected to have an isotopically light signature, as expected from subglacial waters, which could help to explain the temporal differences in isotopic composition of the surface waters.

The differences between early and late summer in AM are less pronounced, most likely owing to the lower primary productivity within the fjord and the steep salinity gradient. However, there are some small-scale differences that could be indicative of changes in meltwater input. There were greater glacial melt proportions combined with higher DSi concentrations in surface waters at AM10 and AM7 in 2018, compared to 2019 (Table 1, Figure S4 in Supporting Information S1). This is the opposite to NK and again highlights the contrasting processes between the fjords. Productivity in AM is relatively low, likely due to the limitation of macronutrients, as there is no upwelling of nutrient rich bottom waters from buoyant submarine plumes, unlike in fjords with marine-terminating glaciers (Meire et al., 2017). Therefore, the DSi concentrations and isotopic composition are more likely a direct indicator of glacial inputs, without such complexity in the isotopic fingerprint from diatom utilisation. So, the higher DSi concentrations further down-fjord in July compared to September potentially reflects peak meltwater input into the fjord from Narssap Sermia, compared to September when meltwater fluxes are lower, although we must note that physical contributions from wind mixing events can also play a role in the distribution of waters within these fjord environments.

#### 4.2.2. Exchange Between Fjord and Coastal Waters

The opposite trends in the relationship between DSi and isotopic composition between the two fjords highlight the heterogeneity of fjord environments and the complexity of upscaling to wider fjord environments. However, such subtle changes in the fjord biogeochemical cycling between the early- and late-summer season may not be critical when considering the overall trend of isotopically light Si within these systems, due to the timescales involved in exchange between fjord and coastal waters. Radium (Ra) isotope geochemistry can be used to trace the fate of lithogenically sourced solutes, due to its similar source (continuous production from thorium) and known decay rates. The shortest-lived Ra isotope ( $^{224}\text{Ra}$ ) has a half-life ( $\lambda$ ) of 3.66 days and showed no correlation with salinity at coastal waters sites sampled at the shelf-break, suggesting that the export of material occurs on longer timescales than can be resolved by this isotope (i.e.,  $>20$  days; Hendry et al., 2019). There was a weak but significant correlation between  $^{223}\text{Ra}$  and salinity (Hendry et al., 2019), the persistence of which suggests a transit time of not more than 2–3 months between the terrestrial source within the fjords and the coastal environment.

This demonstrates a relatively slow exchange between fjord and coastal waters, which suggests changes between early and late summer are less important when considering the role of glacial meltwaters beyond the fjord environment.

## 5. Conclusions

We use silicon isotope geochemistry to highlight that the role of glacial meltwaters in two Greenlandic fjords goes beyond the delivery of rapidly drawn down DSi to surface waters. We demonstrate that fjord environments actively modify coastal waters, resulting in isotopically deplete surface waters with respect to silicon, both in-fjord and across the shelf break. Our results provide evidence for the dissolution of ASi, and potentially desorption of Si from Fe and Mn phases, within fjords that is then utilized for biological production. Despite these release mechanisms, this biological uptake results in very low DSi concentrations of the waters at the mouth of the fjords suggesting that very little biologically available Si reaches ecosystems further downstream. However, there needs to be a better understanding and quantification of the role of reactive particulate phases in the supply of silica to coastal waters, within the glacially derived sediments that escape into the shelf environments.

While we observe differences in biogeochemical patterns and processes between the contrasting fjords and between time periods, the isotopically light composition of DSI is consistently observed despite decreases in DSI concentration as salinity increases. We also highlight that whilst seasonality is important for in-fjord biogeochemical cycling, such as the timing of diatom blooms, it may be less important when considering the export of material beyond the fjord, considering the relatively slow transport times across the shelf break.

We can use these findings to begin to understand potential export of glacially derived nutrients in fjord environments and beyond, although we recognize that any upscaling attempts require caution considering the complex and heterogeneous nature of fjord environments. However, we highlight the importance of investigating nutrient cycles beyond simple surface concentration data and suggest silicon isotopic geochemistry can provide real insights when attempting to better understand the role of glacial meltwater export on downstream ecosystems, within and even beyond the fjord environments.

### Data Availability Statement

The data used in the study are available from the Pangaea data repository (Hatton et al., 2023) via <https://doi.pangaea.de/10.1594/PANGAEA.930217>.

### References

- Arendt, K. E., Nielsen, T. G., Rysgaard, S., & Tønnesson, K. (2010). Differences in plankton community structure along the Godthåbsfjord, from the Greenland Ice Sheet to offshore waters. *Marine Ecology Progress Series*, 401, 49–62. <https://doi.org/10.3354/meps08368>
- Arrigo, K. R., van Dijken, G. L., Castelao, R. M., Luo, H., Rennermalm, Å. K., Tedesco, M., et al. (2017). Melting glaciers stimulate large summer phytoplankton blooms in southwest Greenland waters. *Geophysical Research Letters*, 44(12), 6278–6285. <https://doi.org/10.1002/2017gl073583>
- Becker, S., Aoyama, M., Woodward, E. M. S., Bakker, K., Coverly, S., Mahaffey, C., & Tanhua, T. (2020). GO-SHIP repeat hydrography nutrient manual: The precise and accurate determination of dissolved inorganic nutrients in seawater, using continuous flow analysis methods. In *Frontiers in marine science* (Vol. 7). <https://doi.org/10.3389/fmars.2020.581790>
- Bhatia, M. P., Waterman, S., Burgess, D. O., Williams, P. L., Bundy, R. M., Mellett, T., & Bertrand, E. M. (2021). Glaciers and nutrients in the Canadian Arctic Archipelago marine system. *Global Biogeochemical Cycles*, 35(8), e2021GB006976. <https://doi.org/10.1029/2021gb006976>
- Brzezinski, M. A., Closset, I., Jones, J. L., de Souza, G. F., & Maden, C. (2021). New constraints on the physical and biological controls on the silicon isotopic composition of the Arctic Ocean. *Frontiers in Marine Science*, 8. <https://doi.org/10.3389/fmars.2021.699762>
- Cape, M. R., Straneo, F., Beird, N., Bundy, R. M., & Charette, M. A. (2019). Nutrient release to oceans from buoyancy-driven upwelling at Greenland tidewater glaciers. *Nature Geoscience*, 12(1), 34–39. <https://doi.org/10.1038/s41561-018-0268-4>
- Carmack, E. C., Macdonald, R. W., & Jasper, S. (2004). Phytoplankton productivity on the Canadian shelf of the Beaufort Sea. *Marine Ecology Progress Series*, 277, 37–50. <https://doi.org/10.3354/meps277037>
- Deborde, J., Anschutz, P., Etcheber, H., Commarieu, M., Lacroart, P., & Abril, G. (2007). The dynamics of phosphorus in turbid estuarine systems: Example of the Gironde estuary (France). *Limnology and Oceanography*, 52(2), 862–872. <https://doi.org/10.4319/lo.2007.52.2.0862>
- de la Rocha, C. L., Brzezinski, M. A., & DeNiro, M. J. (1997). Fractionation of silicon isotopes by marine diatoms during biogenic silica formation. *Geochimica et Cosmochimica Acta*, 61(23), 5051–5056. [https://doi.org/10.1016/S0016-7037\(97\)00300-1](https://doi.org/10.1016/S0016-7037(97)00300-1)
- Delstanche, S., Opfergelt, S., Cardinal, D., Elsass, F., André, L., & Delvaux, B. (2009). Silicon isotopic fractionation during adsorption of aqueous monosilicic acid onto iron oxide. *Geochimica et Cosmochimica Acta*, 73(4), 923–934. <https://doi.org/10.1016/j.gca.2008.11.014>
- DeMaster, D. J. (1981). The supply and accumulation of silica in the marine environment. *Geochimica et Cosmochimica Acta*, 45(10), 1715–1732. [https://doi.org/10.1016/0016-7037\(81\)90006-5](https://doi.org/10.1016/0016-7037(81)90006-5)
- de Souza, G. F., Reynolds, B. C., Rickli, J., Frank, M., Saito, M. A., Gerringa, L. J. A., & Bourdon, B. (2012). Southern Ocean control of silicon stable isotope distribution in the deep Atlantic Ocean. *Global Biogeochemical Cycles*, 26(2), GB2035. <https://doi.org/10.1029/2011GB004141>
- Forster, P., Storelvmo, T., Armour, K., Collins, W., Dufresne, J.-L., Frame, D., et al. (2021). The Earth's Energy budget, climate feedbacks, and climate sensitivity. In V. Masson-Delmotte, P. Zhai, A. Pirani, S. L. Connors, C. Péan, S. Berger, et al. (Eds.), *Climate change 2021: The physical science basis. Contribution of working Group I to the sixth assessment report of the intergovernmental panel on climate change* (pp. 923–1054). Cambridge University Press. <https://doi.org/10.1017/9781009157896.009>
- Georg, R. B., Reynolds, B. C., Frank, M., & Halliday, A. N. (2006). New sample preparation techniques for the determination of Si isotopic compositions using MC-ICPMS. *Chemical Geology*, 235(1), 95–104. <https://doi.org/10.1016/j.chemgeo.2006.06.006>
- Giesbrecht, K. E., & Varela, D. E. (2021). Summertime biogenic silica production and silicon limitation in the Pacific Arctic region from 2006 to 2016. *Global Biogeochemical Cycles*, 35(1), e2020GB006629. <https://doi.org/10.1029/2020GB006629>
- Grasse, P., Brzezinski, M. A., Cardinal, D., De Souza, G. F., Andersson, P., Closset, I., et al. (2017). GEOTRACES inter-calibration of the stable silicon isotope composition of dissolved silicic acid in seawater. *Journal of Analytical Atomic Spectrometry*, 32(3), 562–578. <https://doi.org/10.1039/c6ja00302h>
- Grønkjær, P., Nielsen, K. V., Zoccarato, G., Meire, L., Rysgaard, S., & Hedeholm, R. B. (2019). Feeding ecology of capelin (*Mallotus villosus*) in a fjord impacted by glacial meltwater (Godthåbsfjord, Greenland). *Polar Biology*, 42(1), 81–98. <https://doi.org/10.1007/s00300-018-2400-8>
- Hatton, J. E., Hendry, K. R., Hawkings, J. R., Wadham, J. L., Benning, L. G., Blukis, R., et al. (2021). Physical weathering by glaciers enhances silicon mobilisation and isotopic fractionation. *Geochemical Perspectives Letters*, 19, 7–12. <https://doi.org/10.7185/geochemlet.2126>
- Hatton, J. E., Hendry, K. R., Hawkings, J. R., Wadham, J. L., Kohler, T. J., Stibal, M., et al. (2019a). Investigation of subglacial weathering under the Greenland Ice Sheet using silicon isotopes. *Geochimica et Cosmochimica Acta*, 247, 191–206. <https://doi.org/10.1016/j.gca.2018.12.033>
- Hatton, J. E., Hendry, K. R., Hawkings, J. R., Wadham, J. L., Opfergelt, S., Kohler, T. J., et al. (2019b). Silicon isotopes in Arctic and sub-Arctic glacial meltwaters: The role of subglacial weathering in the silicon cycle. *Proceedings of the Royal Society A: Mathematical, Physical and Engineering Sciences*, 475(2228), 20190098. <https://doi.org/10.1098/rspa.2019.0098>

### Acknowledgments

The authors thank all involved in fieldwork during the 2018 and 2019 field campaigns, particularly the crews of the KISAQ and TULU and logistical support from GINR. We also thank the Bristol Isotope Group for ongoing analytical support. JEH and KRH and the fieldwork were funded by UK Royal Society Enhancement Award (RGF/EA181036) and ERC Starting Grant ICY-LAB (678371).

- Hatton, J. E., Ng, H. C., Beaton, A., Hawkings, J., Leng, M. J., Meire, L., et al. (2023). Hydrographic and biogeochemical data from Godthåbsfjord and Ameralik fjord, SW Greenland, 2018–2019 [Dataset]. PANGAEA. <https://doi.org/10.1594/PANGAEA.930217>
- Hawkings, J. R. (2021). Trickle and treat? The critical role of marine-terminating glaciers as icy macronutrient pumps in polar regions. *Journal of Geophysical Research: Biogeosciences*, 126(10), e2021JG006598. <https://doi.org/10.1029/2021JG006598>
- Hawkings, J. R., Wadham, J. L., Benning, L. G., Hendry, K. R., Tranter, M., Tedstone, A., et al. (2017). Ice sheets as a missing source of silica to the polar oceans. *Nature Communications*, 8(1), 14198. <https://doi.org/10.1038/ncomms14198>
- Hendry, K. R., Huvenne, V. A. I., Robinson, L. F., Annett, A., Badger, M., Jacobel, A. W., et al. (2019). The biogeochemical impact of glacial meltwater from Southwest Greenland. *Progress in Oceanography*, 176, 102126. <https://doi.org/10.1016/j.poccean.2019.102126>
- Hopwood, M. J., Bacon, S., Arendt, K., Connelly, D. P., & Statham, P. J. (2015). Glacial meltwater from Greenland is not likely to be an important source of Fe to the North Atlantic. *Biogeochemistry*, 124(1), 1–11. <https://doi.org/10.1007/s10533-015-0091-6>
- Hopwood, M. J., Carroll, D., Dunse, T., Hodson, A., Holding, J., Iriarte, J., et al. (2019). Review Article: How does glacier discharge affect marine biogeochemistry and primary production in the Arctic? *The Cryosphere Discussions*, 14(4), 1347–1383. <https://doi.org/10.5194/tc-2019-136>
- Hopwood, M. J., Carroll, D., Dunse, T., Hodson, A., Holding, J. M., Iriarte, J. L., et al. (2020). Review article: How does glacier discharge affect marine biogeochemistry and primary production in the Arctic? In *Cryosphere* (Vol. 14, No. (4), pp. 1347–1383). Copernicus GmbH. <https://doi.org/10.5194/tc-14-1347-2020>
- Hughes, H. J., Delvigne, C., Kornthuer, M., de Jong, J., André, L., & Cardinal, D. (2011). Controlling the mass bias introduced by anionic and organic matrices in silicon isotopic measurements by MC-ICP-MS. *Journal of Analytical Atomic Spectrometry*, 26(9), 1892–1896. <https://doi.org/10.1039/C1JA10110B>
- Juul-Pedersen, T., Arendt, K. E., Mortensen, J., Blicher, M. E., Sjøgaard, D. H., & Rysgaard, S. (2015). Seasonal and interannual phytoplankton production in a sub-Arctic tidewater outlet glacier fjord, SW Greenland. *Marine Ecology Progress Series*, 524, 27–38. <https://doi.org/10.3354/meps11174>
- Krause, J. W., Schulz, I. K., Rowe, K. A., Dobbins, W., Winding, M. H. S., Sejr, M. K., et al. (2019). Silicic acid limitation drives bloom termination and potential carbon sequestration in an Arctic bloom. *Scientific Reports*, 9(1), 8149. <https://doi.org/10.1038/s41598-019-44587-4>
- Krawczyk, D. W., Witkowski, A., Wanek, J. J., Wroniecki, M., & Harff, J. (2014). Description of diatoms from the Southwest to West Greenland coastal and open marine waters. *Polar Biology*, 37(11), 1589–1606. <https://doi.org/10.1007/s00300-014-1546-2>
- Martin, J. B., Pain, A. J., Martin, E. E., Rahman, S., & Ackerman, P. (2020). Comparisons of nutrients exported from Greenlandic glacial and deglaciated watersheds. *Global Biogeochemical Cycles*, 34(12), e2020GB006661. <https://doi.org/10.1029/2020GB006661>
- Meire, L., Meire, P., Struyf, E., Krawczyk, D. W., Arendt, K. E., Yde, J. C., et al. (2016). High export of dissolved silica from the Greenland Ice Sheet. *Geophysical Research Letters*, 43(17), 9173–9182. <https://doi.org/10.1002/2016GL070191>
- Meire, L., Mortensen, J., Meire, P., Juul-Pedersen, T., Sejr, M. K., Rysgaard, S., et al. (2017). Marine-terminating glaciers sustain high productivity in Greenland fjords. *Global Change Biology*, 23(12), 5344–5357. <https://doi.org/10.1111/gcb.13801>
- Michalopoulos, P., & Aller, R. C. (2004). Early diagenesis of biogenic silica in the Amazon delta: Alteration, authigenic clay formation, and storage. *Geochimica et Cosmochimica Acta*, 68(5), 1061–1085. <https://doi.org/10.1016/j.gca.2003.07.018>
- Mortensen, J., Lennert, K., Bendtsen, J., & Rysgaard, S. (2011). Heat sources for glacial melt in a sub-Arctic fjord (Godthåbsfjord) in contact with the Greenland Ice Sheet. *Journal of Geophysical Research*, 116(1), C01013. <https://doi.org/10.1029/2010JC006528>
- Mortensen, J., Rysgaard, S., Arendt, K. E., Juul-Pedersen, T., Sjøgaard, D. H., Bendtsen, J., & Meire, L. (2018). Local coastal water masses control heat levels in a west Greenland tidewater outlet glacier fjord. *Journal of Geophysical Research: Oceans*, 123(11), 8068–8083. <https://doi.org/10.1029/2018JC014549>
- Mortensen, J., Rysgaard, S., Bendtsen, J., Lennert, K., Kanzow, T., Lund, H., & Meire, L. (2020). Subglacial discharge and its down-fjord transformation in West Greenland Fjords with an ice Mélange. *Journal of Geophysical Research: Oceans*, 125(9), e2020JC016301. <https://doi.org/10.1029/2020JC016301>
- Mortensen, J., Rysgaard, S., Winding, M. H. S., Juul-Pedersen, T., Arendt, K. E., Lund, H., et al. (2022). Multidecadal water mass dynamics on the West Greenland shelf. *Journal of Geophysical Research: Oceans*, 127(7), e2022JC018724. <https://doi.org/10.1029/2022JC018724>
- Ng, H. C., Cassarino, L., Pickering, R. A., Woodward, E. M. S., Hammond, S. J., & Hendry, K. R. (2020). Sediment efflux of silicon on the Greenland margin and implications for the marine silicon cycle. *Earth and Planetary Science Letters*, 529, 115877. <https://doi.org/10.1016/j.epsl.2019.115877>
- Ng, H. C., Hawkings, J. R., Bertrand, S., Summers, B. A., Sieber, M., Conway, T. M., et al. (2022). Benthic dissolved silicon and iron cycling at glaciated Patagonian fjord heads. *Global Biogeochemical Cycles*, 36(11), e2022GB007493. <https://doi.org/10.1029/2022GB007493>
- Oliver, H., Luo, H., Castella, R. M., van Dijken, G. L., Mattingly, K. S., Rosen, J. J., et al. (2018). Exploring the potential impact of Greenland meltwater on stratification, photosynthetically active radiation, and primary production in the Labrador Sea. *Journal of Geophysical Research: Oceans*, 123(4), 2570–2591. <https://doi.org/10.1002/2018jc013802>
- Pickering, R. A., Cassarino, L., Hendry, K. R., Wang, X. L., Maiti, K., & Krause, J. W. (2020). Using stable isotopes to disentangle marine sedimentary signals in reactive silicon pools. *Geophysical Research Letters*, 47(15), e2020GL087877. <https://doi.org/10.1029/2020GL087877>
- Reynolds, B. C., Georg, R. B., Oberli, F., Wiechert, U., & Halliday, A. N. (2006). Re-assessment of silicon isotope reference materials using high-resolution multi-collector ICP-MS. *Journal of Analytical Atomic Spectrometry*, 21(3), 266–269. <https://doi.org/10.1039/B515908C>
- Rysgaard, S., Boone, W., Carlson, D., Sejr, M. K., Bendtsen, J., Juul-Pedersen, T., et al. (2020). An updated view on water masses on the pan-west Greenland continental shelf and their link to proglacial fjords. *Journal of Geophysical Research: Oceans*, 125(2), e2019JC015564. <https://doi.org/10.1029/2019JC015564>
- Santos-García, M., Ganeshram, R. S., Tuerena, R. E., Debyser, M. C. F., Husum, K., Assmy, P., & Hop, H. (2022). Nitrate isotope investigations reveal future impacts of climate change on nitrogen inputs and cycling in Arctic fjords: Kongsfjorden and Rijpfjorden (Svalbard). *Biogeosciences*, 19(24), 5973–6002. <https://doi.org/10.5194/bg-19-5973-2022>
- Stuart-Lee, A. E., Mortensen, J., van der Kaaden, A.-S., & Meire, L. (2021). Seasonal hydrography of Ameralik: A southwest Greenland fjord impacted by a land-terminating glacier. *Journal of Geophysical Research: Oceans*, 126(12), e2021JC017552. <https://doi.org/10.1029/2021JC017552>
- Sutton, J. N., de Souza, G. F., García-Ibáñez, M. I., & De La Rocha, C. L. (2018). The silicon stable isotope distribution along the GEOVIDE section (GEOTRACES GA-01) of the North Atlantic Ocean. *Biogeosciences*, 15(18), 5663–5676. <https://doi.org/10.5194/bg-15-5663-2018>
- Sutton, J. N., Varela, D. E., Brzezinski, M. A., & Beucher, C. P. (2013). Species-dependent silicon isotope fractionation by marine diatoms. *Geochimica et Cosmochimica Acta*, 104, 300–309. <https://doi.org/10.1016/j.gca.2012.10.057>
- Varela, D. E., Pride, C. J., & Brzezinski, M. A. (2004). Biological fractionation of silicon isotopes in Southern Ocean surface waters. *Global Biogeochemical Cycles*, 18(1), GB1047. <https://doi.org/10.1029/2003GB002140>

- Vick-Majors, T. J., Michaud, A. B., Skidmore, M. L., Turetta, C., Barbante, C., Christner, B. C., et al. (2020). Biogeochemical connectivity between freshwater ecosystems beneath the west Antarctic ice sheet and the sub-ice marine environment. *Global Biogeochemical Cycles*, 34(3), e2019GB006446. <https://doi.org/10.1029/2019GB006446>
- Ward, J. P. J., Hendry, K. R., Arndt, S., Faust, J. C., Freitas, F. S., Henley, S. F., et al. (2022). Stable silicon isotopes uncover a mineralogical control on the benthic silicon cycle in the Arctic Barents Sea. *Geochimica et Cosmochimica Acta*, 329, 206–230. <https://doi.org/10.1016/j.gca.2022.05.005>
- Williams, P. L., Burgess, D. O., Waterman, S., Roberts, M., Bertrand, E. M., & Bhatia, M. P. (2021). Nutrient and carbon export from a tidewater glacier to the coastal ocean in the Canadian Arctic archipelago. *Journal of Geophysical Research: Biogeosciences*, 126(9), e2021JG006289. <https://doi.org/10.1029/2021JG006289>
- Woodward, E. M. S., & Rees, A. P. (2001). Nutrient distributions in an anticyclonic eddy in the northeast Atlantic Ocean, with reference to nanomolar ammonium concentrations. *Deep Sea Research Part II: Topical Studies in Oceanography*, 48(4), 775–793. [https://doi.org/10.1016/S0967-0645\(00\)00097-7](https://doi.org/10.1016/S0967-0645(00)00097-7)